JOURNAL OF SOLID STATE CHEMISTRY 37, 232–241 (1981)

An Electron Microscopic Examination of VF_2

HARRY A. EICK

Department of Chemistry, Michigan State University, East Lansing, Michigan 48824

AND LEROY EYRING

Department of Chemistry, Arizona State University, Tempe, Arizona 85281

Received December 31, 1979; in revised form September 10, 1980

Samples of blue and black VF_2, the latter prepared by heating blue VF_2 with VF_3 in a sealed crucible, were examined in the electron microscope. A nonintegral superstructure pattern was observed. Evidence presented supports the hypothesis that this superstructure results from the epitaxial growth of a phase, possibly an oxide, on the surface of the black VF_2, and upon that of both the blue and black forms of VF_2 in a twinned mode upon electron beam irradiation. The capability of the microscope to facilitate explanation of these unexpected results is discussed.

Introduction

Vanadium difluoride, which exhibits the rutile structure, is reported to be colored either light blue or bright gray (*1–3*). When blue crystalline VF_2 is heated with green VF_3, the blue crystals turn black, but the lattice parameters of the VF_2 phase do not change significantly. The blue- or gray-colored material is regarded as the stoichiometric form; the exact composition of the black material, based on X-ray powder and magnetic data is very close to F/V = 2.0 (*4*). The phase VOF and slightly more oxygen-rich oxide–fluoride compositions in which the vanadium oxidation number is slightly higher than +3 and which have been produced under mild pressure retain the rutile structure and are black (*5*). The rutile lattice parameters change from a = 4.797 Å, c = 3.251 Å for VF_2 to a = 4.618 Å c = 3.011 Å for VOF, an indication that the lattice parameter is a moderately sensitive indicator of composition (*2, 5*).

Homologous series of intermediate phases which exist between Ti_2O_3 (sometimes doped with other first-row transition metal atoms) and rutile-type TiO_2 have been elucidated by means of extensive electron microscopic studies (*6–10*). Since VF_2 is isostructural with TiO_2, it seemed that, by application of this technique, any subtle structural changes responsible for the color difference in these apparently otherwise identical vanadium fluoride phases might be identified and explained. One major difference between this study and those involving titanium is the fact that Ti(IV) is rela-

0022-4596/81/050232-10$02.00/0

tively easily reduced; V(II) is not. We present below the results of an electron microscopic study of blue and black VF_2.

Experimental

Crystals of blue and black VF_2 were provided by W. O. J. Boo of the University of Mississippi. The black crystals had been prepared by sealing an equimolar mixture of blue VF_2 and green VF_3 into an evacuated molybdenum crucible by electron beam welding. The crucible was heated by induction at a temperature below the fusion point of VF_3 (1395°C) for ~30 hr (*3*). Black VF_2 and green VF_3 crystals in the product were separated manually. Prior to their use for this study the crystals had been confined in stoppered plastic vials for ~6 years.

Samples of the crystals to which annealed ThO_2 (a = 5.59525 ± 5 Å) or Pt (a = 3.9237 ± 3 Å) had been added as an internal standard were examined by X-ray diffraction on a Guinier 114.59-mm camera (Cu$K\alpha$ radiation) and lattice parameters were determined by a linear-regression procedure (*11*). The crystals were then crushed extensively under liquid nitrogen, and an acetone slurry of the pulverized material was placed on a holey carbon grid. The crystals were examined on a JEM 100B transmission electron microscope operated at 100 kV. The techniques used have been described previously (*12*). The following rutile-type zones were examined: [100],[1] [110], [101], [111], [112], [103], [210], [201], [211], [212], [213], [310], [311], and [312], in addition to two others which were not identified. Distances on the electron diffraction patterns were converted to reciprocal lattice spacings by comparison with the interplanar spacings calculated for VF_2 reflections from the accepted lattice parameters (*2*). Mean distances, together with their standard deviations, are presented when measurement could be effected on more than one photograph. Lattice image fringe spacings were converted to direct lattice vectors by applying a magnification factor of 500,000×.

[1] All symbols which relate to unit cells refer to the rutile structure.

Results

Guinier X-ray diffraction patterns of the black and the blue VF_2 specimens revealed the following lattice parameters. For black VF_2, a = 4.798 ± 0.002 Å, c = 3.231 ± 0.001 Å, for blue VF_2, a = 4.803 ± 0.001 Å, c = 3.2358 ± 0.0005 Å. The errors reported are the standard deviations of the least-squares refinement. An overexposed X-ray diffraction pattern of the black VF_2 crystals exhibited some diffuse lines which are presented in Table I. The strongest reflection listed in the table was weak compared to VF_2 reflections.

Most, but not all, of the electron diffraction patterns from crystals of black VF_2 showed a nonintegral superstructure along {011} in zones [100], [111], [211], [212], and [311] (see Figs. 1 and 2, in which electron diffraction patterns of zones [111] and [100]

TABLE I

REFLECTIONS IN AN OVEREXPOSED X-RAY DIFFRACTION PATTERN OF BLACK VF_2 NOT ASSIGNABLE TO EITHER VF_2 OR VF_3[a]

$\sin^2\Theta$	Interplanar d value (Å)	Intensity
0.01943	5.526	s
0.02611	4.767	m–s
0.03900	3.900	m
0.04264	3.730	m
0.04866	3.492	broad
0.05856	3.183	vw
0.08629	2.622	vw
0.08791	2.598	vvw
0.09922	2.445	w
0.1669	1.885	vvw

[a] Cu$K\alpha$ radiation.

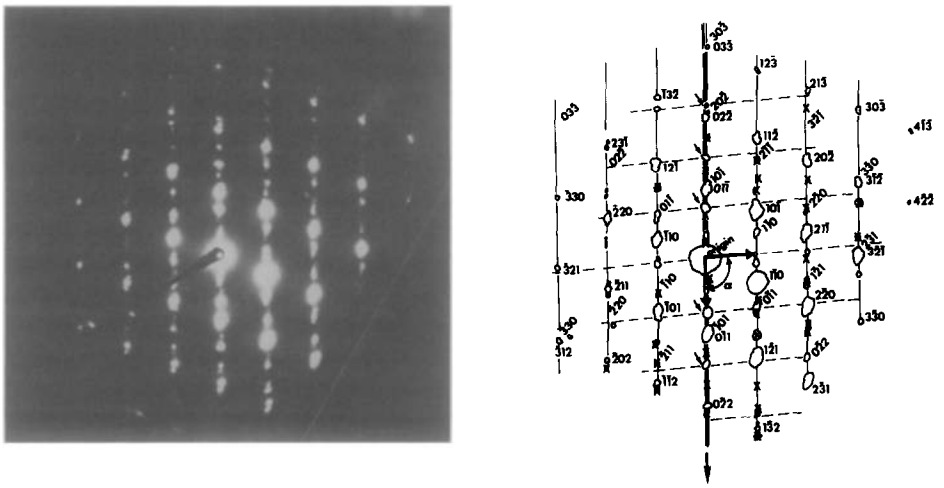

FIG. 1. Electron diffraction pattern of zone [111] from a sample of black VF_2. The zone is interpreted in the adjacent plate. The twin plane along {011} is designated by the triple line. Regular and twin rutile-type indices are designated by the horizontal and slanted indices, respectively. Note the nonintegral reflections coincident with {011} and almost coincident with $\{3\bar{2}\bar{1}\}$, which are assigned to the epitaxial phase. An "x" overlays other reflections which can be assigned to the epitaxial phase as a result of double diffraction. The two vectors describe axes chosen for the epitaxial cell, as described in the text. The arrow indicates the orientation of this figure with that presented in Fig. 2.

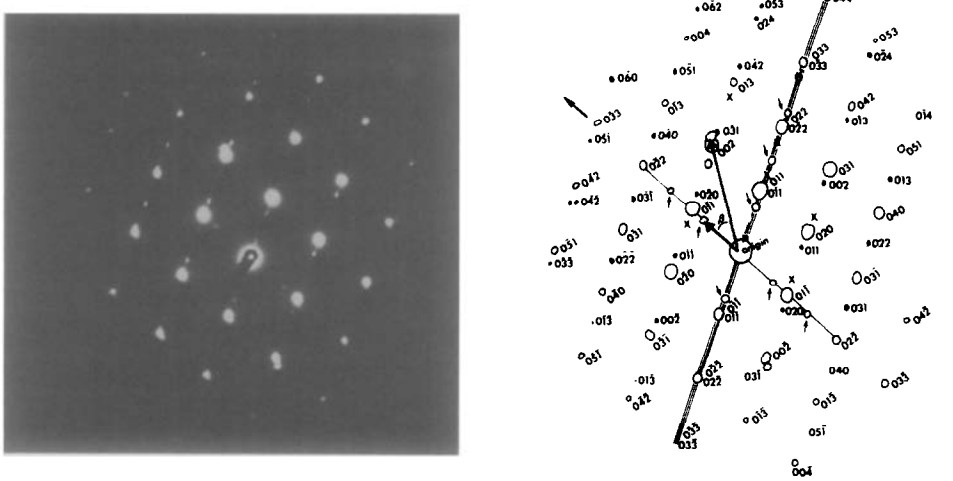

FIG. 2. Electron diffraction pattern of zone [100] from a sample of black VF_2. Rutile-type Miller indices and reflections are indicated in the adjacent plate. The twin plane along {011} is designated by the triple line. Regular (open) and twin (darkened) reflections are designated by the slanted and normal indices, respectively. Nonintegral spacings coincident with {011} are designated by the arrows. The "x" identifies reflections which result from double diffraction. Note the doubling apparent at $(00\bar{2})$ and (002). The two vectors indicate axes chosen for the epitaxial cell, as described in the text.

are presented). One component of the nonintegral spacing apparent in these electron diffraction photographs is a vector ~3.7 Å almost coincident with {011} and 0.73 times as long. Twinning is also apparent. Electron diffraction patterns (zones [100], [110], and [210]) also show a nonintegral superstructure along [002]. In Fig. 3 the zone [110] electron diffraction pattern from a black VF_2 crystal is presented. Reflection (001) which is space group extinct appears in electron diffraction patterns of both blue and black VF_2, probably as a result of double diffraction, as do some other weaker reflections. The doubling of reflections along {002} is particularly apparent and results from a vector, designated "*c*," coincident with and slightly longer than (002). The average length of this vector is 3.00 ± 0.03 Å (from zones [110] and [100]).

Crystals of black VF_2 which did not initially evidence superstructure were found to develop, in the course of normal beam heating,[2] an electron diffraction pattern identical to that found naturally—with the exception that the patterns so produced always evidenced an additional degree of twinning. In beam-heated specimens superstructure was found along both $\{01\bar{1}\}$ and $\{10\bar{1}\}$ in the [111] and [100] zones.

The lattice image photographs are best characterized as a sea of moiré fringes. Most images of zone [110] consisted of only a moiré pattern (Fig. 4) which is characteristic of the difference between the (002) vector and that of the "*c*" vector described previously. Those of zones [100], [111], and [211] were primarily composed of moiré fringes, but either near the edge of thin crystals or in etch pits some images showed a fringe pattern with a repeat distance of ~3.5 Å perpendicular to {011}, and to {101} if twinning were present. In zone [111] (Fig. 5) two vectors, each ~3.5 Å at an angle of ~83.5° to each other, can be identified in the clear image near the crystal edge. The one vector is coincident with $[0\bar{1}1]$; the other is almost, but not quite, coincident with $[3\bar{2}\bar{1}]$, and almost, but not quite, three times its length. This latter vector was evident in the electron diffraction patterns of those zones which showed *h k* permutations of $(3\bar{2}\bar{1})$, i.e., zones [211] and [103]. Image spacings of ~3.5 Å were

[2] The beam heating occurs primarily during high-resolution imaging. The exact temperature to which the specimen is heated is not known, but is believed to be less than 300°C.

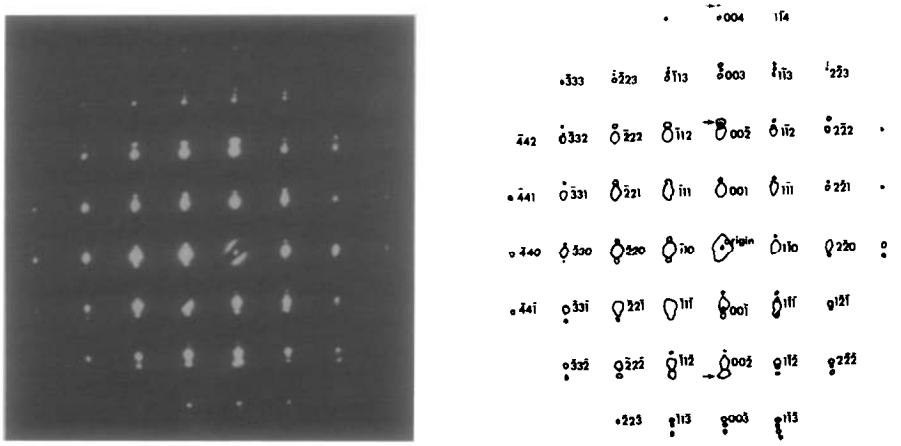

FIG. 3. Electron diffraction pattern of zone [110] from a crystal of black VF_2. Rutile-type Miller indices of reflections are noted in the adjacent plate. The arrows denote a reciprocal lattice vector slightly longer than that of (002).

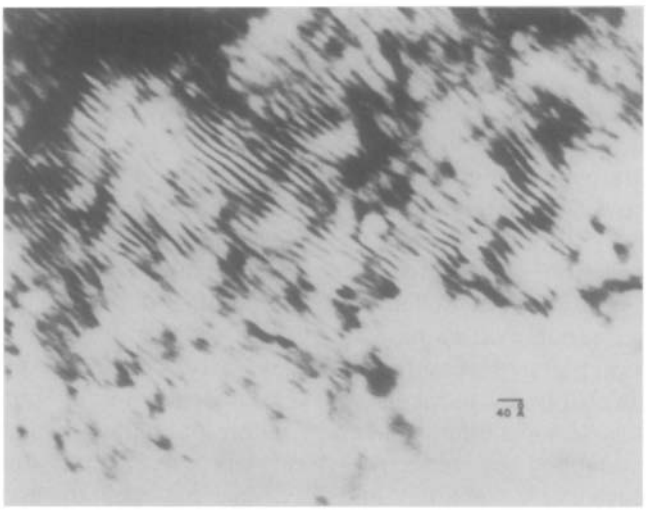

FIG. 4. Lattice image photograph of zone [110], differences in length of the vector to (002) on that of the new phase.

also apparent in a few images of zone [110], and their respective electron diffraction patterns. These spacings apparent in the etch pits in Fig. 6 and in electron diffraction patterns (Fig. 7) can be interpreted as a projection of the vector almost coincident with $[3\bar{2}\bar{1}]$ onto the [110] zone and serve as an indicator that the vector need not lie exactly in the [111] zone. The $\sim 50°$ angle between adjacent extra diffraction spots is reflective of the angle between vectors $[3\bar{2}\bar{1}]$ and $[2\bar{3}1]$.

The excellent quality image photographs of zone [111] (Fig. 5) indicate that the

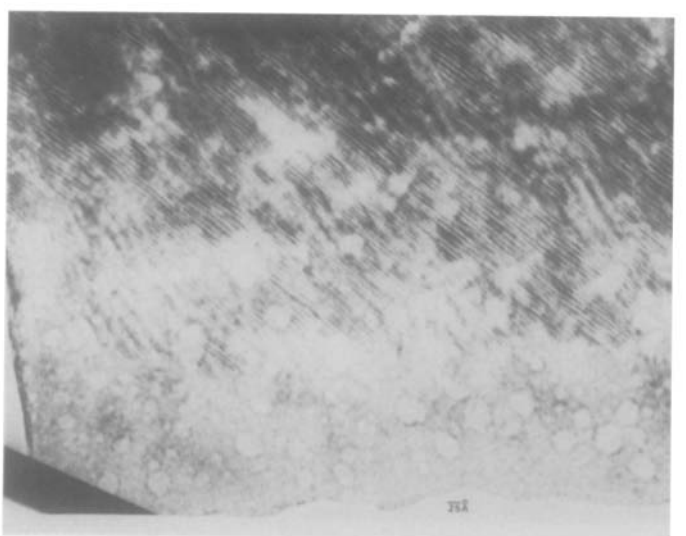

FIG. 5. Lattice image photograph of zone [111], black VF_2. In the enlargement (3.2×) note the distinct fringe pattern of the epitaxial phase near the edge of the crystal.

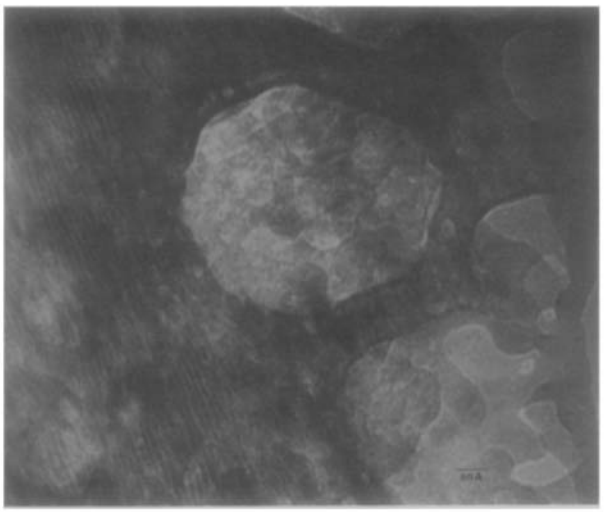

FIG. 6. Lattice image photograph of zone [110], which shows in a circular etch pit spacings of ~3.5 Å characteristic of the epitaxial phase.

distance along $(0\bar{1}1)$ and $(32\bar{1})$ is 3.45 Å. From electron diffraction patterns calibrated as described previously the mean value of the vector coincident with $(0\bar{1}1)$ is 3.67 ± 0.03 Å (from zones [110], [111], and [211]); that of the vector along $(3\bar{2}\bar{1})$ is 3.62 ± 0.06 Å (from zones [111] and [211]). The obtuse angle between these vectors in zones [111] is 96.5°, significantly different from the value of 91.47° calculated for the angle between $(0\bar{1}1)$ and $(3\bar{2}\bar{1})$ from the rutile lattice parameters (*13*).

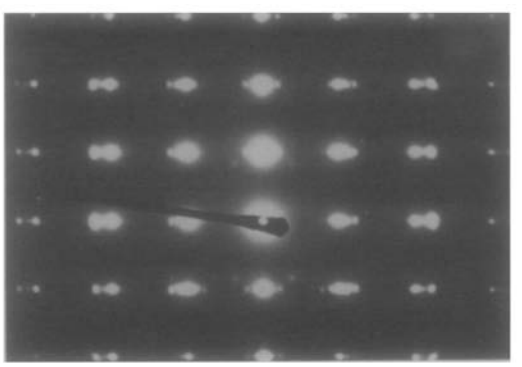

FIG. 7. Electron diffraction pattern of zone [110], black VF_2, which shows spots characteristic of the epitaxial phase. These reflections appear not to lie in this zone and provide evidence that the epitaxial phase can grow at an angle to both the [110] and the [111] zones.

A direct lattice cell can be described in terms of the three vectors which lie either on or adjacent to (002), $(0\bar{1}1)$, and $(3\bar{2}\bar{1})$. The angle between (002) and $(0\bar{1}1)$ in zone [100] is calculated to be 34.1°; that between $(3\bar{2}\bar{1})$ in zone [111] and (002) in zone [100] is 112.3° (*13*). The latter angle clearly has a large associated error since the vector, "*b*," is not coincident with $(3\bar{2}\bar{1})$. On the assumptions that the two vectors observed in the [111] zone are identical, and that the more accurate parameters are derived from the electron diffraction photographs, a triclinic but not necessarily primitive cell can be derived with the following parameters: $a = b = 3.66 \pm 0.08$ Å, $c = 3.00 \pm 0.03$ Å, $\alpha = 112.3°$, $\beta = 34.1°$, $\gamma = 96.5°$.

This triclinic cell is transformed by the program TRACER into another triclinic cell, $a = 3.00$, $b = 3.51$, $c = 2.05$ Å, $\alpha = 102.5°$, $\beta = 90.9°$, $\gamma = 66.1°$ when the error, del (the absolute value of the largest permissible difference between any two of the reduced cell scalar products) is set to 0.1,

an unrealistically small value (*14*). When del is set at the more reasonable value of 0.5, the triclinic cell reduces to a body-centered orthorhombic cell, $a = 3.00$ Å, $b = 6.42$ Å, $c = 2.05$ Å.

Blue VF_2 crystals did not evidence superstructure in their electron diffraction patterns upon initial examination after insertion into the microscope. However, after moderate to intense beam heating they yielded patterns identical to those described above, but always twinned. In Fig. 8 the growth of twins upon beam heating is apparent. Images of these crystals in which the nonintegral reflections appeared as a result of beam heating yielded only spacings expected for VF_2, or moiré fringes.

Pitting, possibly a result of beam degradation, was evident as round spots (see Figs. 5 and 6) in many of the images, as was a herringbone pattern characteristic of twinning (see Fig. 9). Electron diffraction patterns of zones which did not contain the reflections (011), (002), or $(3\bar{2}\bar{1})$, or $h\ k$ permutation thereof, showed only random

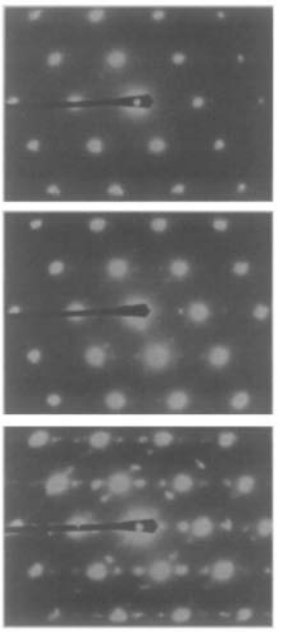

FIG. 8. Electron diffraction patterns of zone [111] of a blue VF_2 crystal which illustrate the growth of twinned reflections from the epitaxial phase upon intense beam heating.

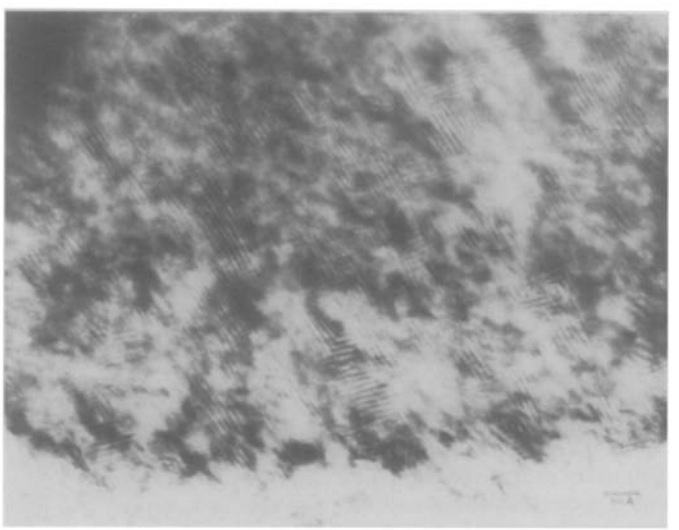

FIG. 9. Lattice image photograph of zone [100] which shows a "herringbone" pattern characteristic of twin formation. The moiré fringes result from the interaction of reflections $(0\bar{1}1)$ and $(\bar{1}01)$ with those of the epitaxial phase.

extra spots, and yielded images with fringes assignable to the rutile structure.

Discussion

The extra reflections in the diffraction pattern, unlike those in TiO_2 and related rutile systems, do not integrally divide the principal rutile reflections. Nor are those reflections which correspond to an observed fringe in the image always collinear with the rutile layer line. For example, in zone [111] (Fig. 1) the vector terminates just to the side of the $(3\bar{2}\bar{1})$ reflection.

The behavior observed can be interpreted in two different ways:

(1) as evidence for an epitaxial surface reaction between the VF_2 crystals and oxygen (or water), forming VF_2O_x; or

(2) as evidence of a bulk reaction in which the same products are formed and are oriented in a manner similar to that of the epitaxial phase with respect to the parent rutile lattice. Either interpretation is consistent with the expected behavior of V(II), which is characteristically easily oxidized, but only difficultly reduced, and then normally to the metal under strong reducing conditions. Either is also consistent with the observed similarity of the X-ray data of the blue and black forms of VF_2. The surface of the black VF_2 crystals may have been oxidized during heating with VF_3, and the outer structure changed slightly, or hydrolyzed or oxidized during storage and a new structure grown epitaxially on the VF_2 surface. It is postulated that the black VF_2 crystals developed color centers during the heating with VF_3, and subsequently oxidized or hydrolyzed during storage, forming the epitaxial layer. The fact that a number of the black crystals show the additional surface-grown structure probably results from the grinding, sampling, and thin-crystal selection process in the microscope. The fact that the epitaxial phase is observed in the images principally in localized areas such as etch pits and near the edge of the crystal is consistent with the higher concentration of this phase in thinner regions of the crystal.

The impact of beam degradation is obvious. Crystallites which exhibit only the rutile structure upon initial beam exposure soon evidence the pattern characteristic of the epitaxial phase. Oxidation (or hydrolysis) of beam-heated samples in the 10^{-5}-Torr atmosphere of the microscope is a common phenomenon. Such behavior has been observed for selected lanthanide compounds (*15, 16*).

The twinned superstructure which developed upon beam heating is also an epitaxial surface reaction. Such twinning is frequently observed in the microscope (*15*). The close relationship between this epitaxial phase and that observed usually untwinned in black VF_2 implies that the two are identical.

The electron diffraction and lattice image photographs provide no difinitive evidence as to the nature of the black phase. The normally extinct (001) in [110] which might substantiate that extra fluorine was present in black VF_2 was equally intense in patterns of both the blue and black phases, and was absent in both phases in [100].

The extra reflections identified in the heavily exposed Guinier photograph were not observed in the Debye–Scherrer photograph taken immediately after sample preparation, but were observed in a severely overexposed Debye–Scherrer photograph taken during the course of this work (*17*). The presence of these extra reflectons is the strongest argument for a bulk oxidized phase. But the phase observed in the electron diffraction and lattice image photographs does not appear to explain them. As a consequence, the extra phase is believed to be the same and epitaxial in both specimens.

All [110] zone images are dominated by moiré fringes. These wavy fringes, whose

spacings correspond to 14–16 Å, result from the difference between the (002) (1.63 Å) spacing and the ~1.50 Å, almost parallel spacings of the epitaxial phase. The waviness, typical of moiré fringes, probably reflects variations in thickness of the surface layer and warping of the crystal. The plethora of spots adjacent to the rutile reflections in this zone probably results from double diffraction. This ~1.50 Å reflection is considered a second order vector of the epitaxial phase even though it cannot be identified directly in any images of the zones in which it is located. It grows into rutile-type electron diffraction patterns upon beam heating, and is always evident in the [110] or [100] zone of crystals which show the ~3.5 Å vector. The problem which results from the absence of a third primitive vector verified in an image as characteristic of the epitaxial cell is discussed later.

The [111] zone images (Fig. 5) yield direct confirmation of two vectors and the subtended angle of the epitaxial surface phase. Within the error limits, these two vectors are of identical length. It is not clear from the electron diffraction photographs of zones [111] and [211] that both vectors lie exactly in the zone. They could be either slightly above or below the zone axis with only the peaks in the zone or could pass through the zone at a shallow angle. The observation of the epitaxial phase in selected [110] zone image photographs implies the latter to be the case. The angle between the [111] zone and the [110] zone is ~46°. Thus, the appearance of the first and second order reflections of the epitaxial phase in some zone [110] electron diffraction patterns (and images) is strong support that the growth of the phase does not bear a fixed relationship to either of these zones. If this is indeed the case the distances determined from the diffraction patterns are projections of the true length and consequently shorter than it.

The extensive streaking along $(01\bar{1})$ in [111] (Fig. 1) and in [100] (Fig. 2) and the herringbone pattern (Fig. 9) are indicative of twinning. In [100] the twinning along (011) which can be regarded as a 180° rotation about the twin axis is designated in the indexing adjacent to the photographs. The zigzag herringbone fringes have a spacing of ~10 Å, with a 70° angle in the pattern. The angle is characteristic of that between the $(0\bar{1}1)$ and the $(10\bar{1})$ reflections; the ~10 Å fringe reflects the differences between the {011} spacing (2.69 Å) and the ~3.6 Å of the epitaxial phase. The same type of twinning, 180° rotation on $[0\bar{1}1]$, is apparent in the [111] zone.

In addition to this twinning about $[0\bar{1}1]$, there is also twinning of the epitaxial phase about [002]. This latter twinning results most frequently from exposure to the electron beam.

The epitaxial phase has been characterized uniquely by three vectors, two verified directly in the image photographs, and the other deduced from the electron diffraction patterns and the moiré fringes of the images. The parameter values reported are those derived from the electron diffraction patterns since for those a common calibrant was used.

The centered orthorhombic cell to which this triclinic cell reduced is unrealistically small (volume = 39.48 Å^3), further indication that the vectors chosen from the lattice images are not primitive. This reduction is tantamount to a fit of $\pm 5 \times 10^{-3}$ in low-angle Q values, a fit probably relatively close to the actual error. That the b (6.42 Å) parameter is two times that of the rutile c axis (3.23 Å) implies this to be a common axis.

Interplanar d spacings calculated from the six observed parameters did not agree with values calculated for expected products, i.e., V_2O_3, VOF_x, etc. Nor did the calculated values match those listed in Table I. There are two reasons for the failure

of such a match. The first is the absence of low-angle reflections. Doubling the various parameters of the reduced orthogonal cell and recalculation of powder patterns did not significantly improve the agreement with d values either calculated for expected oxidation products or listed in Table I. The second factor which makes phase identification difficult is the lack of precision of the parameters of the epitaxial phase. Parameters derived from the electron diffraction patterns differed by up to 0.2 Å from those measured on the image photographs. Such a deviation is not surprising. Since there is evidence that the phase does not always lie parallel to the rutile zone, the error limits are expected to be relatively large, and the true parameters may actually be somewhat larger than those reported.

The capabilities of electron microscopy and diffraction as applied to the solid state have been discussed recently (*18*). This work affords another opportunity to point out the power of the tool in enabling unexpected results to be interpreted.

Acknowledgments

The authors express their gratitude to Mr. John Wheatley of the Center for Solid State Science at Arizona State University; to Professor W. O. J. Boo, University of Mississippi, for providing the samples and the motivation for the research; to a referee for many suggestions; and especially to Professor J. Cowley, Arizona State University, for helpful insights into the problem. Financial support was provided by the National Science Foundation, through Grant DMR77-08473.

References

1. J. W. Stout and W. O. J. Boo, *J. Appl. Phys.* **37,** 966 (1969).
2. C. Cross, R. Feuer, and M. Pouchard, *J. Fluorine Chem.* **3,** 457 (1975).
3. M. W. Shafer, *Mater. Res. Bull.* **4,** 905 (1969).
4. R. F. Williamson and W. O. J. Boo, *Inorg. Chem.* **19,** 31 (1980).
5. B. L. Chamberland, A. W. Sleight, and W. H. Cloud, *J. Solid State Chem.* **2,** 49 (1970).
6. L. A. Bursill and B. G. Hyde, *Acta Crystallogr. Sect. B* **27,** 210 (1971).
7. L. A. Bursill, I. E. Grey, and D. J. Lloyd, *J. Solid State Chem* **16,** 331 (1976).
8. D. K. Philp and L. A. Bursill, *Acta Crystallogr. Sect. A* **30,** 265 (1974).
9. D. K. Philp and L. A. Bursill, *J. Solid State Chem.* **10,** 357 (1974).
10. L. A. Bursill, *J. Solid State Chem.* **10,** 72 (1974).
11. O. Lindquist and F. Wengelin, *Ark. Kemi.* **28,** 179 (1967).
12. S. Iijima, *Acta Crystallogr. Sect. A* **29,** 18 (1973).
13. "International Tables for X-Ray Crystallography," Vol. II., p. 109, Kynoch Press, Birmingham (1959).
14. S. L. Lawton and R. A. Jacobson, "The Reduced Cell and Its Crystallographic Applications," Report IS-1141, Ames Laboratory, Iowa State University of Science and Technology, April, 1965.
15. G. Schiffmacher, *J. Microsc. Spectrosc. Electron.* **2,** 503, (1977).
16. L. Eyring, private communication.
17. W. O. J. Boo, private communication.
18. G. Van Tendeloo, D. Van Dyck, J. Van Landuyt, and S. Amelinckx, *J. Solid State Chem.* **27,** 55 (1979).